PNAS RESEARCH ARTICLE | BIOPHYSICS AND COMPUTATIONAL BIOLOGY

Autoregulation of switching behavior by cellular compartment size

Monika Jozsa[a], Tihol Ivanov Donchev[a], Rodolphe Sepulchre[a], and Timothy O'Leary[a,1]

Edited by Herbert Levine, Northeastern University, Boston, MA; received September 2, 2021; accepted January 24, 2022

Many kinds of cellular compartments comprise decision-making mechanisms that control growth and shrinkage of the compartment in response to external signals. Key examples include synaptic plasticity mechanisms that regulate the size and strength of synapses in the nervous system. However, when synaptic compartments and postsynaptic densities are small, such mechanisms operate in a regime where chemical reactions are discrete and stochastic due to low copy numbers of the species involved. In this regime, fluctuations are large relative to mean concentrations, and inherent discreteness leads to breakdown of mass-action kinetics. Understanding how synapses and other small compartments achieve reliable switching in the low–copy number limit thus remains a key open problem. We propose a self-regulating signaling motif that exploits the breakdown of mass-action kinetics to generate a reliable size-regulated switch. We demonstrate this in simple two- and three-species chemical reaction systems and uncover a key role for inhibitory loops among species in generating switching behavior. This provides an elementary motif that could allow size-dependent regulation in more complex reaction pathways and may explain discrepant experimental results on well-studied biochemical pathways.

synaptic plasticity | dendritic spine | biochemical switch | calcium/calmodulin kinase CaMKII | bistability

Significance

Biochemical reactions often occur in small volumes within a cell, restricting the number of molecules to the hundreds or even tens. At this scale, reactions are discrete and stochastic, making reliable signaling difficult. This paper shows that the transition between discrete, stochastic reactions and macroscopic reactions can be exploited to make a self-regulating switch. This constitutes a previously unidentified kind of reaction network that may be present in small structures, such as synapses.

A switch is a fundamental operation required of biochemical signaling. In essence, a switch is a system that reliably transitions between at least two distinct states while exhibiting a memory, or hysteresis, that preserves the state in the absence of input. Such systems are critical for cellular decision-making processes, including apoptosis (1–3), cell fate decisions (4–6), and synaptic plasticity (7). Much of what we know about switching behavior in these contexts relies on mass-action kinetics that model concentrations of biochemical species as continuous, deterministic quantities (1, 2, 5, 8–11).

However, many cellular compartments, including synaptic spines and postsynaptic densities, contain concentrations of key signaling enzymes that correspond to hundreds or even tens of individual molecules (12, 13) Mass-action kinetics break down in this regime, and even relatively simple biochemical reaction motifs exhibit qualitative changes in behavior as system size transitions between macroscopic and microscopic limits. A famous example includes the so-called toggle switch motif (14), a pair of mutually inhibitory enzymes that, under certain parameter regimes (15, 16), exhibits a single stable equilibrium in the mass-action limit and two distinct stochastic modes in the microscopic limit. This system thus acts as a switch in the small system size/low–molecule count regime that will give way to a single stable equilibrium if system size increases.

In this paper, we put forward the hypothesis that biological systems may exploit the qualitative transition between discrete, stochastic dynamics at the microscopic scale and deterministic, continuous dynamics at the macroscopic limit. Many cellular compartments grow in size, and the growth process itself depends on the outcome of a cellular decision: a switching event. This raises the possibility that system size can act as a feedback signal to self-regulate switching behavior.

Using analysis and simulations of simple reaction motifs, we substantiate this hypothesis with a working model. We show that generic, mutually inhibitory reactions between two or more species can give rise to switch-like behavior in the microscopic limit that gives way to a stable behavior as the system size increases. Furthermore, these systems can regulate the size evolution of small systems using their switch-like behavior, maintain the stability of large systems, and integrate external input that encourages growth.

Our results and hypothesis provide a signaling motif that may be exploited by cellular systems to make growth decisions in a regime where the inherent randomness and discreteness of biochemical signals govern the dynamics.

Author affiliations: [a]Department of Engineering, University of Cambridge, CB2 1PZ Cambridge, United Kingdom

Author contributions: T.O. designed research; M.J., T.I.D., R.S., and T.O. performed research; M.J. and T.I.D. analyzed data; and M.J., T.I.D., and T.O. wrote the paper.

The authors declare no competing interest.

This article is a PNAS Direct Submission.

[1]To whom correspondence may be addressed. Email: timothy.oleary@eng.cam.ac.uk.

This article contains supporting information online at https://www.pnas.org/lookup/suppl/doi:10.1073/pnas.2116054119/-/DCSupplemental.

Published March 29, 2022.

A Size-Dependent Stochastic Switch Motif

We begin by exploring simple reaction networks that exhibit size-dependent bistability; the system behaves as a switch when the total number of molecules is low (in the tens) and has a single stable equilibrium as system size increases. Our goal is not to model any specific reaction pathway in detail but to characterize minimal motifs of two or three reacting species that can support switching behavior. Such motifs may constitute building blocks or subnetworks that confer switching functionality to more complex chemical reaction networks, including those governing synaptic plasticity and growth of synaptic densities (12).

A well-studied motif (14–17), shown in Fig. 1*A*, is a pair of mutually inhibitory species, x_1 and x_2, described by the differential equations

$$\frac{d\left(\frac{x_j}{n}\right)}{dt} = \frac{k}{k+\left(\frac{x_i}{n}\right)} - \frac{k\left(\frac{x_j}{n}\right)}{k+1}, \quad i,j=1,2, i\neq j \qquad [1]$$

corresponding to the reaction scheme [where $\mathbf{x}=(x_1,x_2)$]:

$$x_1 \xrightarrow{\lambda_{x_1}(\mathbf{x})=\frac{kn}{k+\left(\frac{x_2}{n}\right)}} x_1+1 \qquad x_1 \xrightarrow{\mu_{x_1}(\mathbf{x})=\frac{kn\left(\frac{x_1}{n}\right)}{k+1}} x_1-1$$

$$x_2 \xrightarrow{\lambda_{x_2}(\mathbf{x})=\frac{kn}{k+\left(\frac{x_1}{n}\right)}} x_2+1 \qquad x_2 \xrightarrow{\mu_{x_2}(\mathbf{x})=\frac{kn\left(\frac{x_2}{n}\right)}{k+1}} x_2-1. \qquad [2]$$

A key feature of this system is that the prediction of the classical kinetics Eq. **1** deviates from the stochastic modeling framework (18) when the population size of x_1 or x_2 is small. As we will see, this feature is closely linked to the different behavior of the system with small and large system sizes.

The deterministic model Eq. **1** describes the time evolution of the species x_1 and x_2 normalized by a parameter n, where (n,n) is the steady state (unique stable equilibrium) of the system, as depicted in Fig. 1*B*. This model is a good description of how chemical reaction systems behave in the macroscopic (mass-action) limit where reactant abundance can be reasonably modeled as continuous concentrations. However, in small cellular compartments with reactants present in low copy numbers, reactions are discrete and stochastic, so the evolution of (x_1,x_2) corresponds to a birth–death process, as defined in Eq. **2**. Thus, to faithfully model system behavior in microscopic limits throughout this paper, we adopt this stochastic modeling framework and use Gillespie's algorithm (19) for numerical simulations (*SI Appendix*). We call the parameter n defined above the size of the system because it represents the expected number of molecules at equilibrium in the classical (mean-field) limit (Eq. **1**).

In the stochastic, discrete case, Eq. **2** describes the time evolution of x_1 and x_2 as integer numbers of molecules. Strikingly, when n is small and the total count of $\mathbf{x}$ is in the tens, the stochastic model dwells into two distinct modes close to the axes, as illustrated in Fig. 1*C* (15, 16). When n is large, x_1 and x_2 fluctuate around n, and thus, Eq. **1** predicts the average behavior of the birth–death process. This illustrates the qualitative difference in behavior of the same reaction motif in the microscopic and macroscopic limits.

In Eq. **2**, species x_2 inhibits the production of x_1 by reducing its birth rate λ_{x_1} and vice versa via standard Michaelis–Menten dynamics (ref. 20, appendix A). Both species catalyze their own degradation with death rates μ_{x_1},μ_{x_2}. This system is derived from the well-known toggle switch, originally used as a model of mutually repressing gene transcripts in genetically engineered *Escherichia coli* (14, 17). These original studies assumed that there is steep cooperativity in the birth rates of each species, resulting in two stable equilibria in the deterministic framework that describe a bistable, macroscopic, mean-field behavior (also known as mass-action kinetics). Such systems have switching behavior for any system size. As opposed to the toggle switch in refs. 14 and 17, the noncooperative birth–death process Eq. **2** with a single stable equilibrium of its deterministic description Eq. **1** allows for both stable and switch-like behavior depending on the copy numbers of the species.

To better understand this dual behavior, we will show that the stationary probability distribution (*SI Appendix*) $P^s(\mathbf{x})$ of system Eq. **2** has one or more modes depending on the parameters n and k. When n is large, $P^s(\mathbf{x})$ has one mode with its peak being around $\bar{\mathbf{x}}=(n,n)$. This means that $\bar{\mathbf{x}}$ is an attractor point around which the process fluctuates. When n is small, $P^s(\mathbf{x})$ is bimodal where the two mode peaks lie along the two axes. This distribution describes a switching behavior of the system Eq. **2** between the two modes. The appearance of bimodality happens due to transient extinction of one of the species that becomes a prevailing phenomenon in the low-number regime.

Our key insight is that a biological system may exploit this size-dependent behavior to regulate its own size. Specifically, if the switch itself triggers growth, then we have a feedback mechanism between the behavior (switching or nonswitching) and the system size. This constitutes a form of self-regulation that permits growth at small sizes and then, annihilates switching behavior above

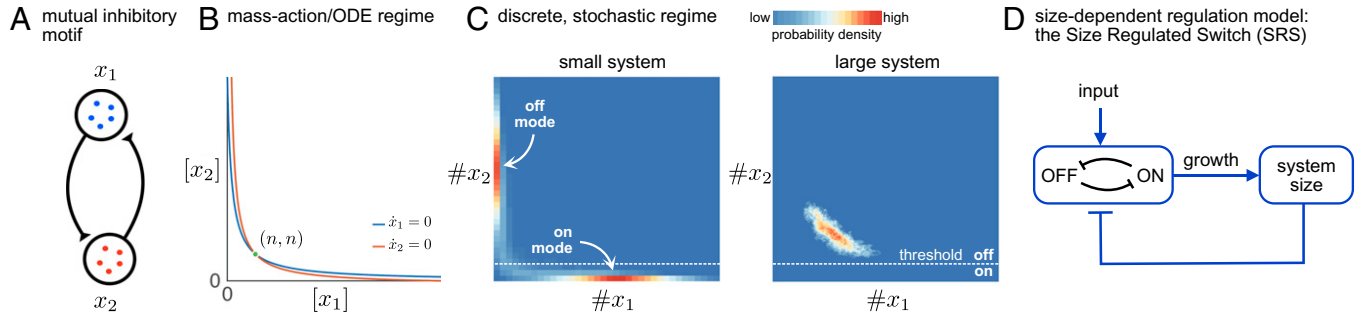

Fig. 1. (*A*) Schematic of a system with mutually inhibitory interactions between two species. (*B*) Phase plane and nullclines of the deterministic ordinary differential equation (ODE) model of the mutual inhibiting system (Eq. **1**), showing a unique (stable) fixed point at the intersection of the nullclines, $\dot{x}_1=0;\dot{x}_2=0$. (*C*) Illustration of the stochastic, discrete version of the mutually inhibiting system. Probability densities are plotted as a function of species count, $\#x_1,\#x_2$, with red shades indicating high probability and blue indicating low probability. For small system size n, there are two distinct modes, which we label ON and OFF; for large system size, there is only one mode close to the fixed point of the deterministic ODE model. In this specific case, we depict the switch threshold such that low copy numbers of x_2 correspond to an ON state and vice versa. (*D*) Diagram of our proposed mechanism—the SRS—that exploits the switch behavior of the stochastic, discrete system to autoregulate growth.

a size threshold. We call such a system a size-regulated switch (SRS). Fig. 1*D* illustrates this idea; input can push the switch into the ON state, triggering growth. Once the system reaches a critical size, it will lose bimodality/switching behavior and dwell away from the ON state (as depicted in Fig. 1*C*). We next demonstrate this idea with a simple model of synaptic potentiation and growth that allows the strength of an external signal to determine whether a small, immature synapse will grow and stabilize.

Synapse Size as a Regulator of Synaptic Plasticity

Synaptic transmission depends on neurotransmitter binding to receptors in small biochemical structures called postsynaptic densities. In many types of excitatory synapses, synapse strength is partly regulated by active processes that remodel the synapse and increase its size and strength in response to external signals, including strong excitatory input that elevates calcium concentration in the vicinity of the postsynaptic density (PSD). Calcium influx, in turn, triggers biochemical pathways that have long been hypothesized to exhibit switch-like or threshold behavior (21, 22).

In excitatory synapses, the postsynaptic site is often compartmentalized in a spine, a small membrane protrusion with a volume typically less than 1 μm^3. The development and maintenance of synaptic contacts and of spine volume are governed by a host of biochemical signaling events (12, 23), the most extensively studied being activity-dependent plasticity mechanisms—long-term potentiation and depression—that are coupled to growth and retraction of the synapse, respectively (22, 24–27). Widespread experimental evidence points to several consistent features of excitatory plasticity and associated structural changes in dendritic spines.

- Potentiation mechanisms implement a threshold on excitatory signals and accompanying calcium influx, resulting in a switch-like decision to potentiate (22, 24–27).
- Potentiation (increase in receptor count) is strongly coupled to growth of the dendritic spine, resulting in a direct correlation between synapse strength and compartment size (28, 29).
- Small synapses are more susceptible to being potentiated or depressed (and eliminated); as synapses increase in size and strength, their capacity to potentiate further is reduced (30–34).
- The size of dendritic spines is positively correlated to the age and life expectancy of the spine (35).
- Much of the signaling machinery involved in this process involves enzymes that are present in concentrations at the nanomolar to micromolar range. Thus, while large spines can contain hundreds or thousands of enzyme molecules, nascent spines (sometimes called filopodia) likely restrict these numbers to the tens or less (12, 13).

These observations mean it is likely that synapse growth involves a transition between microscopic and macroscopic biochemical signaling. Furthermore, they imply a biochemical switching mechanism that operates reliably in the low-number/high-noise regime and that becomes less sensitive as the number of signaling molecules in the postsynaptic compartment increases. We should stress that dendritic spines are not the smallest identifiable compartment in a (post-)synapse. The PSD is an elaborate protein complex that houses postsynaptic receptors, scaffolding proteins, kinases, and other molecular machinery that regulates synaptic transmission (12, 23, 36, 37). Moreover, PSD size correlates with synaptic strength by virtue of its role in anchoring neurotransmitter receptors (38). Thus, one may consider the PSD as the relevant compartment in which size-dependent regulation occurs.

Several decades of experimental work have identified candidate switching networks (9, 12, 39), most notably those involving calcium–calmodulin/calcium-calmodulin-dependent protein kinase II (CaMKII) (7, 21, 22, 39). To date, the interpretation of these studies remains controversial, with some evidence suggesting an absence of bistability (26, 40) and other work indicating that switching is context dependent (27) or that switching deactivates rapidly following dendritic spine growth (25).

We next outline a mechanism for synaptic spine evolution that captures the key phenomena enumerated above. We will neglect the effect of diffusion within the compartment in which the switch operates; we are thus assuming the system is well mixed. This may be reasonable if the reaction rates are slow relative to diffusion times. Studies have shown that macromolecules can diffuse across dendritic spines on a millisecond timescale (41–43), which is negligible relative to the time window during which synaptic plasticity occurs (25, 44). However, many signaling molecules do not diffuse freely—particularly those in the PSD (36). In this case and as we alluded to above, it may be more reasonable to interpret local confined clusters of interacting proteins and possibly, the PSD itself as the relevant compartment.

We introduce an input signal to the two-species system Eq. **2** and couple the states where switching occurs to growth and shrinkage processes. This provides a generic model of a biochemical switch in a cellular compartment, such as a dendritic spine. As we will show, this results in a form of self-regulation that allows the system to operate reliably as a switch in the low-number regime and that gives way to a stable behavior as size increases.

An SRS Motif for Synapse Growth. As we showed previously, the two-species system Eq. **2** has three possible modes: one around the mean-field equilibrium in the large size limit and two along the axes in small systems. We now introduce feedback between the modes and system size via a simple growth model, resulting in an SRS model of synapse evolution as depicted in Fig. 2*A*. Without loss of generality, we assume that the mode along axis x_1 is the ON mode, triggering growth, and the mode on axis x_2 is the OFF mode, triggering shrinkage. When the process is in the growth or shrinkage mode, the size parameter n increases or decreases in proportion to the time that the process spends in the corresponding mode. The third mode around the macroscopic equilibrium is assigned to be the rest mode; hence, when the process is in that mode, n does not change. For the purpose of this control mechanism on n, the mode boundaries are defined simply based on the concentration of the species; we say that the process $\mathbf{x}(t) = (x_1(t), x_2(t))^T$ is in growth mode at time t if the concentration of x_1 is larger than 75% [i.e., when $x_1(t)/(x_1(t) + x_2(t)) > 0.75$]. By symmetry, the process is in shrinkage mode if $x_2(t)/(x_1(t) + x_2(t)) > 0.75$. Otherwise, the process is in rest mode. Note that the results can easily be extended for other choices of mode boundaries.

As described above, the modes of the SRS on the axes represent mechanisms of shrinkage and growth: that is, the size n of an SRS process dynamically increases or decreases depending on which mode the process is in. When n decreases to zero, we eliminate the synapse. As n increases, the modes along the axes become smaller and shift farther along the axes. In addition, the system gradually forms a third mode around $\bar{\mathbf{x}} = (n, n)$ corresponding to

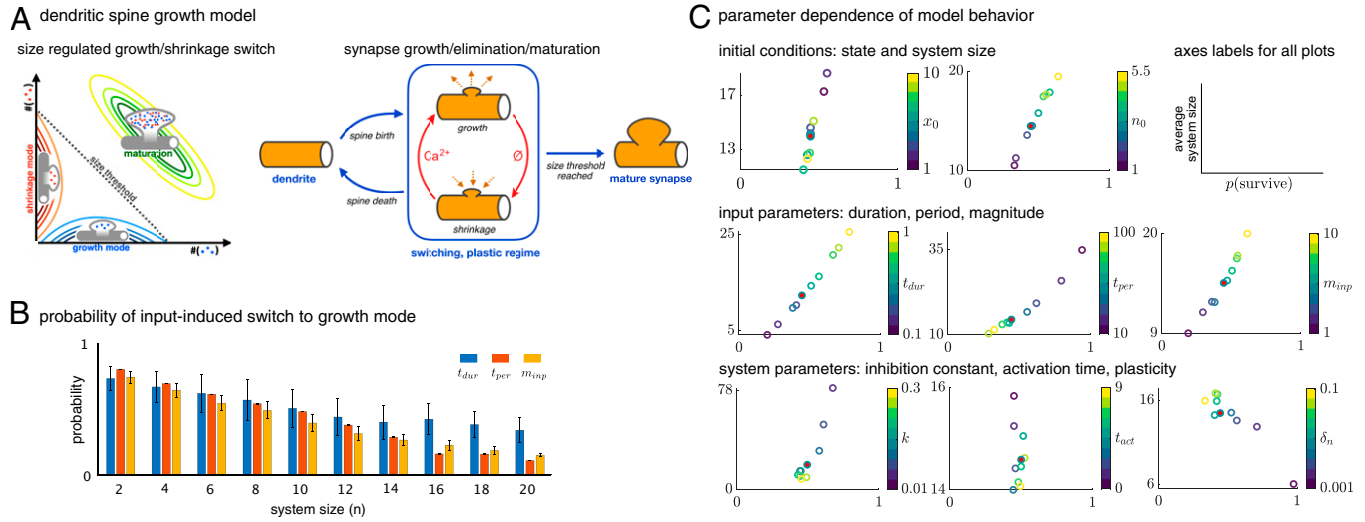

Fig. 2. A model of dendritic spine growth. (*A*) A schematic of the SRS model of dendritic spine growth. (*B*) Input sensitivity of SRS for different system sizes. As the system size increases, the SRS is less likely to switch from shrinkage mode to growth mode. This applies for a wide range of input parameters (e.g., changing t_{dur} and fixed t_{per}, m_{inp}; blue boxes). More details are in *SI Appendix*. (*C*) Survival probability vs. average system size for varying parameters. Points filled with red denote the baseline parametrization. The parameters, in particular the input parameters (*Middle*), can tune both the average system size and the survival probability. The system parameters (*Bottom*) are less suitable for tuning survival probability than the input parameters.

the rest mode. Eventually, when n grows large enough, the system becomes unimodal, with the rest mode being its only mode.* Thus, it becomes a stable system.

We next introduce two parameters to couple the shrinkage and growth modes to system size. First, we define a mode activation time threshold t_{act}. A mode will be active and thus, have an effect on the system size when the process is in that mode for longer than t_{act} time. Second, we use a plasticity constant δ_n that determines how much the system size changes when the process is in shrinkage or growth mode. When a mode is active, change in the system size is applied after every reaction in the following way; if the present time is t and τ time passed since the last reaction, then the new system size is given by $n(t) = n(t-\tau) \pm \delta_n \tau$, where the plus/minus sign is determined by the type of mode.

We extend the SRS by adding an excitatory input that encourages the evolution of the process toward the growth mode. For simplicity, this input is chosen to be periodic; however, other input types are expected to lead to similar results if their role is to bias the evolution of the process toward the growth mode. To describe the periodic input, we use three parameters: 1) the period between inputs t_{per}, 2) the duration of the input $t_{\text{dur}} < t_{\text{per}}$, and 3) the magnitude of the input m_{inp}. With this, the effect of the input is as follows; when $t \in (mt_{\text{per}}, mt_{\text{per}} + t_{\text{dur}})$ for $m = 1, 2, \ldots$, then the birth rate λ_{x_1} of x_1 is modified to $\lambda_{x_1} + m_{\text{inp}}$.

In addition to the parameters of the mode effects and the input, the SRS is described by the initial conditions $\mathbf{x}(0) = (x_0, x_0)$ and $n(0)$ and a constant k parameter that is inversely related to the inhibition strength between x_1 and x_2 (Eq. **2**). Note that the shapes of the modes depend on k, which then affects the magnitude of fluctuation in the modes, the average dwell time, and the probability of switching within a time interval. More details are in *SI Appendix*.

To probe the behavior of the SRS, we analyzed the survival probability and the size evolution under a range of conditions. Results are shown in Fig. 2 *B* and *C*. We fixed a baseline parametrization $(x_0, n_0, k, t_{\text{act}}, \delta_n, t_{\text{per}}, t_{\text{dur}}, m_{\text{inp}})$ of the SRS and defined a set of values (values of interest) around the baseline value for each parameter $(I_{x_0}, I_{n_0}, I_k, I_{t_{\text{act}}}, I_{\delta_n}, I_{t_{\text{per}}}, I_{t_{\text{dur}}}, I_{m_{\text{inp}}})$. To show how the parameters affect the behavior of the system, we changed the parameters one by one within their values of interest while holding the other parameters at their baseline values. For each of these parameterizations, we simulated the SRS and estimated the survival probability p_{surv} of the system as the proportion of survived processes among all realizations and the average system size $\bar{n}$ averaged over time and realizations (Fig. 2*C*). In each plot, a point shows the number of the survived processes of 100 realizations against the average system size (averaged over time and realizations).

The input parameters $m_{\text{inp}}, t_{\text{per}}, t_{\text{dur}}$ affect p_{surv} and $\bar{n}$ as expected; when the input is stronger, both p_{surv} and $\bar{n}$ increase. Note that the input can be strengthened in three ways; it can have larger magnitude, shorter period, or longer duration. From the near-linear relationship between these input features and p_{surv} and $\bar{n}$, we conclude that the input can finely tune both p_{surv} and $\bar{n}$.

With increasing the plasticity parameter δ_n, the system size n becomes more volatile, and thus, reaching $n = 0$ becomes more probable. This results in a smaller p_{surv}. However, a more volatile system induces a larger average size $\bar{n}$ due to the bias toward growth from the applied input. In parallel, longer activation time threshold t_{act} slightly decreases $\bar{n}$ as it weakens plasticity.

The results on parameter k show that stronger inhibition (smaller k) induces larger $\bar{n}$ and p_{surv}. This agrees with the observations on the system Eq. **2** that for smaller k parameters, the modes are farther along the axes for the following reason. When modes are farther along the axes, they are also farther apart from each other; thus, switching occurs less, and the input-induced bias toward growth applies more. Note that for small-enough k, the process is likely to stay in one mode within the timescale that we simulated.

Finally, the results on the initial conditions x_0 and n_0 reveal that a system with larger system size has higher survival probability and is more likely to grow bigger. The initial state x_0 has a weaker but opposite effect. This is because when x_0 is farther from the axes, the processes need more time to get to the modes along the axes, and thus, it takes longer for the system size n to evolve.

*The modes along the axes are magnitudes smaller and are far along the axes so that the process is guaranteed to stay in the rest mode for the time of interest. Note that in principle, if time is infinite, the process can visit the practically inaccessible growth and shrinkage modes, and since (0, 0) is an absorbing state, the process eventually dies.

To sum up, the SRS provides a stochastic switching mechanism that controls system size in a manner analogous to the potentiation of dendritic spines. The sensitivity and behavior of this control mechanism can be easily tuned through parameters, such as the inhibition strength (k) between the species and plasticity parameters (t_{act}, δ_n). Furthermore, external input determines system size (synapse size) and survival probability in qualitative agreement with experimental observations; smaller spines get potentiated more easily than larger spines (30–34), and the expected lifetime of smaller spines (smaller n_0) is shorter (35).

Generalization of the System

Our results so far indicate that a regulated switch can be readily implemented in a very simple and ubiquitous motif consisting of two mutually inhibitory chemical species. Such a mechanism may underlie synaptic structural plasticity and other cellular decision-making processes that involve growth and signaling with small numbers of molecules. However, the specific system we have focused on is unlikely to exist in its precise form in any biological system for the simple reason that most biochemical signaling networks involve a multitude of species and exhibit diversity in their architectures and kinetic parameters. We, therefore, asked to what extent a size-regulated switching mechanism can generalize to multiple species and to the addition of excitatory coupling between the species.

Two-Species Switching Systems. To begin with, we generalize the two-species system by introducing excitation between species besides inhibition and by allowing asymmetry in interaction strengths. We thus consider three types of birth–death processes $\mathbf{x}(t) = (x_1(t), x_2(t))$: 1) type S_{II}, where the two components x_1 and x_2 mutually inhibit each other; 2) type S_{IE}, where x_1 excites x_2 and x_2 inhibits x_1; and 3) type S_{EE}, where the two components mutually excite each other. For all three cases, at any time instant, x_1 and x_2 increase or decrease by one in the next infinitesimal time interval with a probability proportional to the corresponding birth rates $[\lambda_{x_1}(\mathbf{x}), \lambda_{x_2}(\mathbf{x})]$ and death rates $[\mu_{x_1}(\mathbf{x}), \mu_{x_2}(\mathbf{x})]$. This evolution is described as follows:

$$\begin{aligned} x_1 &\xrightarrow{\lambda_{x_1}(\mathbf{x})} x_1 + 1 \qquad x_1 \xrightarrow{\mu_{x_1}(\mathbf{x})} x_1 - 1 \\ x_2 &\xrightarrow{\lambda_{x_2}(\mathbf{x})} x_2 + 1 \qquad x_2 \xrightarrow{\mu_{x_2}(\mathbf{x})} x_2 - 1, \end{aligned} \qquad [3]$$

where the reaction rates

$$\begin{aligned} \lambda_{x_i}(\mathbf{x}) &= \frac{k_{ji}\bar{x}_i}{k_{21} + \frac{x_j}{\bar{x}_j}}, \quad \mu_{x_i}(\mathbf{x}) = \frac{k_{ji}x_1}{k_{ji}+1} \text{ if } x_j \text{ inhibits } x_i \\ \lambda_{x_i}(\mathbf{x}) &= \frac{\bar{x}_i\frac{x_j}{\bar{x}_j}}{k_{ji} + \frac{x_j}{\bar{x}_j}}, \quad \mu_{x_i}(\mathbf{x}) = \frac{x_i}{k_{ji}+1}, \text{ if } x_j \text{ excites } x_i \end{aligned} \qquad [4]$$

are based on standard models in biochemistry (ref. 20, appendix A). Note that in our simulations, we perturbed the rates corresponding to the excitatory connections to allow the systems S_{EE} to revive from the origin (*SI Appendix*).

The birth and death rates are described by the parameters k_{12}, k_{21} and $\bar{x}_1, \bar{x}_2$. The parameters k_{ij}, $i, j = 1, 2, i \neq j$ determine the strength of inhibition or excitation of x_i by x_j. Analogous to the previous section, the parameters $\bar{\mathbf{x}} = (\bar{x}_1, \bar{x}_2)$ define a unique state where the birth and death rates are in balance [i.e., $\lambda_{x_i}(\bar{\mathbf{x}}) = \mu_{x_i}(\bar{\mathbf{x}})$ for $i = 1, 2$], providing an equilibrium of the mean-field description of Eq. **3** given by

$$\frac{dx_j}{dt} = \lambda_{x_j}(\mathbf{x}) - \mu_{x_j}(\mathbf{x}), \quad j = 1, 2. \qquad [5]$$

For simplicity, throughout this paper, we will assume that $\bar{x}_1 = \bar{x}_2 = n$, and we will call n the system size as in previous sections. Note that the analysis can be extended to the general case. We focus on systems where $\bar{\mathbf{x}} = (n, n)$ defines a unique, stable equilibrium of Eq. **5**. In general, if $\bar{x}_1$ and $\bar{x}_2$ are larger than some threshold, which depends on the parameters k_{12} and k_{21}, the birth–death process fluctuates around $\bar{\mathbf{x}}$ (ref. 45, chapter 10). However, when either $\bar{x}_1$ or $\bar{x}_2$ is small, other attractor points may arise. Examples of S_{II}, S_{IE}, and S_{EE} processes and their stationary distributions for these two regimes are illustrated in Fig. 3. The columns correspond to the three types S_{II}, S_{IE}, and S_{EE}, and the rows correspond to systems with small (Fig. 3, *Upper*) and large (Fig. 3, *Lower*) system size n.

Modality of the stationary distribution is a key feature for describing the behavior of stochastic systems. A unimodal biochemical system acts like a noisy stable system, and thus, it is suitable for static functionality. A multimodal biochemical system, on the other hand, acts like a switch operator, and thus, it is suitable for dynamic functionality.

To understand the functionality of S_{II}, S_{IE}, and S_{EE} systems, we detected the parameter regimes for unimodality and multimodality by empirically calculating the probability mass corresponding to the largest mode of the stationary probability distributions. We call this probability the largest mode weight (LMW). When the LMW is close to one, the system is unimodal, and when it is significantly smaller than one, the system is multimodal. For calculating the LMW, we applied our mode search algorithm (*SI Appendix*) that identifies the modes and the corresponding probability masses of empirical stationary probability distributions.

In Fig. 4, we show the LMW of symmetric ($k_{12} = k_{21}$) (Fig. 4, *Upper*) and asymmetric ($k_{12} \neq k_{21}$) (Fig. 4, *Lower*) S_{II}, S_{IE}, and S_{EE} systems for a range of parameters k_{12}, k_{21}, and n (*SI Appendix* has more details on the parameters). As we can see, the S_{II} system acquired both unimodality (yellow regions) and multimodality (dark regions) for a significant range of parameter triples (k_{12}, k_{22}, n). Before discussing this interesting phenomenon, we summarize the results for the other two types

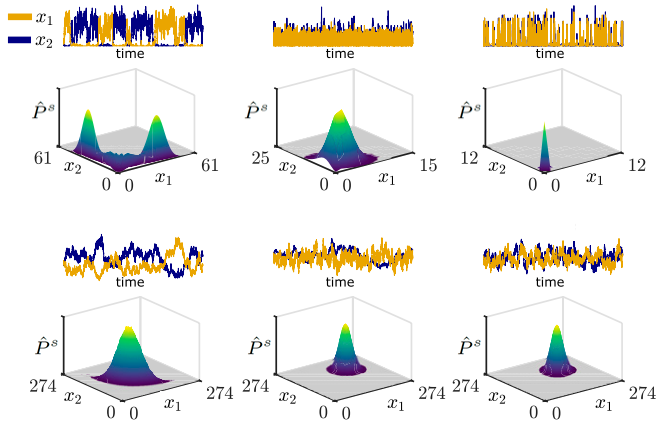

Fig. 3. Examples of empirical stationary distributions $\hat{P}^s$ of type S_{II}, S_{IE}, and S_{EE} systems (from left to right, respectively) with $k_{12} = k_{21} = 0.1$ and small $n = 2$ (*Upper*) and large system sizes $n = 100$ (*Lower*). Robust multimodality appears only for S_{II} systems with small system size n. Segments of the corresponding processes are depicted above the distributions.

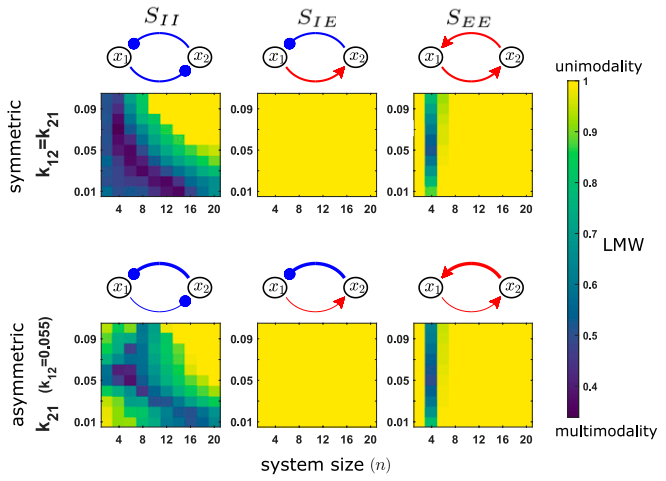

Fig. 4. Size-dependent modality (transition from dark to yellow) typifies fully inhibitory systems (S_{II}) where it is robust to asymmetry and to the strength of inhibition. This can be seen from the LMW of the empirical stationary distributions corresponding to symmetric ($k_{12} = k_{21}$; *Upper*) and asymmetric ($k_{12} \neq k_{21}$; *Lower*) systems S_{II}, S_{IE}, and S_{EE} (from left to right). Graphs above the heat maps illustrate the connectivities (blue: inhibition; red: excitation; thickness of the lines: connectivity strength).

of systems shown in Fig. 4, *Center* and *Right*; S_{IE} systems are unimodal for all parameters considered, whereas S_{EE} systems showed multimodality besides unimodality for a narrow range of parameters. This fragile multimodality of S_{EE} systems can be described as follows. The stationary distribution of S_{EE} systems has a single sharp mode at $(0, 0)$ for small n, representing a complete death of the species, a more spread out single mode near $\bar{x}$ for large n, and a mixture of these latter two modes for a few intermediate values of n. This type of multimodality is out of the interest of this paper for two reasons. 1) A mode corresponding to the death of the species is not suitable for dynamic functionality (e.g., it has no relevance in a feedback mechanism such as the SRS). 2) This multimodality is not robust in the parameters and thus, less relevant biologically.[†]

In contrast to type S_{IE} and S_{EE} systems, when S_{II} is multimodal, its modes appear at nontrivial states away from the origin. In the symmetric case, when $k = k_{12} = k_{21}$, the system is multimodal for small and unimodal for large system sizes. The transition between these two happens gradually and for different system sizes depending on k (stronger inhibition—smaller k—widens the parameter regime of multimodality). In the asymmetric case, the system starts as a unimodal system (except for nearly symmetric cases), transits to multimodality for some intermediate system sizes, and transits back to unimodality for large system sizes.

Analysis of Network Properties That Facilitate Size-Dependent Switching. The previous results suggest that S_{II} systems have the unique feature of developing multimodality in the small system size regime that is robust for all parameters (k_{12}, k_{21}, n). To what extent does this hold more generally? We sought a means to quantify the key property of mutually inhibitory species that underlies this capacity for switching by analyzing the linearized fluctuations of the system. Such a method could open up the possibility to explore size-dependent multimodality of larger reaction networks, a possibility we will explore in three-species systems.

In general, there is no known analytic solution for stationary distributions of state-dependent nonlinear birth–death processes (15). The most accurate approximations are gained by simulating the birth–death processes and calculating the empirical distributions. However, these simulations are computationally expensive and thus, do not scale well with the number of parameters (values for k and n) or with the number of species in the system. Furthermore, simulations alone restrict the amount of insight that can be gleaned from results. To address this, we used an analytical approximation, the linear noise approximation (LNA) (45), that approximates the distribution up to second order. More precisely, in the LNA method, a system is approximated by a Fokker–Plank equation, whose stationary distribution is a multivariate Gaussian distribution with mean $\bar{x}$ and covariance matrix Σ (*SI Appendix*). In the case of multimodal distributions, this Gaussian distribution does not provide a reasonable approximation; however, as we will show, some fundamental properties of the systems, such as the direction of the fluctuations, are captured by this approximation. Moreover, the Gaussian distribution approximation can give insights to the modality of the original systems through the introduction of a measure.

We can quantify the fluctuations of birth–death processes by calculating the covariance matrix Σ from the LNA. Graphically, for a two-species system, the covariance matrix is represented in the state plane by an ellipse centered at the mean of the distribution. Fig. 5 shows the shape of the ellipses of representative symmetric systems for S_{II}, S_{IE}, and S_{EE}. In the S_{EE}-type systems, species tend to increase or decrease simultaneously, resulting in covariances with positive correlation. The ellipses representing the covariances of S_{IE} systems are close to a circle. On the other hand, S_{II}-type systems have negative correlation, representing a competition between the species. When the S_{II} systems have bimodal distributions (Fig. 5) (values of LMW that are significantly smaller than one), the linearization exhibits fluctuations that largely exceed the positive orthant. Since the number of molecules cannot be negative, this excess tends to concentrate on the axis of the positive orthant, predicting the bimodal behavior in the original system. As the system transitions to unimodal distribution (LMW tending to one), the excess outside the positive orthant of Gaussian approximation decreases. With these observations in mind, we investigate to what extent a modality can be predicted merely from the linearized system.

To gain insight of the modality prior to simulating data, we introduce a measure using the Gaussian distribution resulted from the LNA. This measure is the probability mass of the Gaussian distribution in the positive orthant, denoted by P_{in}. Fig. 5 shows that the value of P_{in} is directly related to that of the LMW and

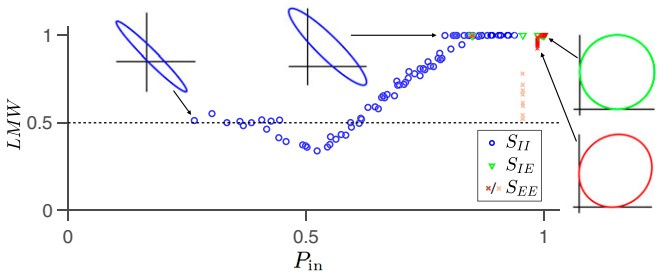

Fig. 5. P_{in} provides a reliable insight of the system's modality for systems with two species. The scatterplot illustrates the relationship between the LMW of the empirical distribution and the probability mass of the Gaussian distribution from the LNA inside the positive orthant (P_{in}) for S_{II}-, S_{IE}-, and S_{EE}-type systems and parameters $k \in [0.03, 0.1]$ and $n \in [2, 20]$. Note that the "weak" bimodality of the S_{EE} type due to the $(0, 0)$ mode (highlighted as pink crosses) is not captured by the LNA method. The ellipses attached to the extremal points in the scatterplot represent the corresponding Gaussian approximation of the fluctuations.

[†]The sharpness of $(0, 0)$ and the size of the intermediate n depend on the perturbation on the excitatory connection discussed in *SI Appendix*.

therefore, to the behavior of the original system. Note that the outlier pink crosses correspond to the bimodal S_{EE} systems where one of the modes peaks at $(0, 0)$, and thus, for the reason discussed earlier, they are out of the interest of this paper.

In the next section, we investigate the modality of systems with three species. It will be shown that for three-dimensional systems, P_{in} can give a hint for modality and for the tendency of modality as n changes. In essence, the direction of the covariance is captured well by the LNA, which makes it a good indicator whether size-dependent multimodality appears in a system. However, the magnitude of the fluctuation of multimodal systems is largely underestimated by the LNA, which sets limitations in detecting the parameter regimes for the different modalities (*SI Appendix*).

Three-Species Switching Systems. As emphasized previously, the biological relevance of our results depends on a switch being implementable in a more general reaction network. We have seen that among the two-species systems that we considered, the mutual inhibitory system S_{II} robustly acquires multimodality for small system sizes. Furthermore, as the system size grows, the systems transit from multimodality to unimodality. We also showed that multimodality can often be predicted by negative correlation in the fluctuations of the species at the equilibrium, obtained from the LNA. We sought to test the generality of these findings in simulation. However, with the growth of the number of species, simulations quickly become intractable because both the volume of the parameter space and the support of the probability distribution of the systems grow exponentially. We, therefore, examined the extent to which our findings generalize from two- to three-dimensional systems.

Consider the time evolution of three chemical species $\mathbf{x}(t) = (x_1(t), x_2(t), x_3(t))$, where each species may influence the evolution of the others by inhibiting or exciting their growth. Denote the connectivity matrix between the species describing these relations by $C \in \{1, 0, -1\}^{3\times 3}$, where

$$C_{ij} = \begin{cases} 1, \text{ if } x_i \text{ excites } x_j \\ -1, \text{ if } x_i \text{ inhibits } x_j \\ 0 \text{ species } x_i \text{ does not influence species } x_j \end{cases} \quad [6]$$

for $i, j \in \{1, 2, 3\}$, $i \neq j$. Then, the system evolves according to the following reaction scheme:

$$x_i \xrightarrow{\lambda_{x_i}(\mathbf{x})} x_i + 1 \qquad x_i \xrightarrow{\mu_{x_i}(\mathbf{x})} x_i - 1, \quad [7]$$

where the birth λ_{x_i} and death μ_{x_i} rates of a species x_i, $i \in \{1, 2, 3\}$ are given by

$$\lambda_{x_i}(\mathbf{x}) = \sum_{j:C_{ji}=-1} \frac{k_{ji}\bar{x}_i}{k_{21} + x_j/\bar{x}_j} + \sum_{j:C_{ji}=1} \frac{\omega\bar{x}_i x_j/\bar{x}_j}{k_{ji} + x_j/\bar{x}_j}$$

$$\mu_{x_i}(\mathbf{x}) = \left(\sum_{j:C_{ji}=-1} \frac{k_{ji}}{k_{21}+1} + \sum_{j:C_{ji}=-1} \frac{\omega}{k_{21}+1} \right) x_i$$

for some ω, k_{ij}, and $\bar{x}_i$ constants. Parallel to previous sections, we assume that $\bar{x}_1 = \bar{x}_2 = \bar{x}_3 = n$, and we call n the system size. Note that $\bar{\mathbf{x}} = (\bar{x}_1, \bar{x}_2, \bar{x}_3)$ defines a unique equilibrium state of the macroscopic equations (Eq. **5**) that guarantees the stationary distribution to be unimodal for large n (ref. 45, chapter 10).‡

‡The excitatory connections are perturbed for the simulations similar to the two-species systems (*SI Appendix*), which guarantees the uniqueness of equilibrium $\bar{\mathbf{x}}$.

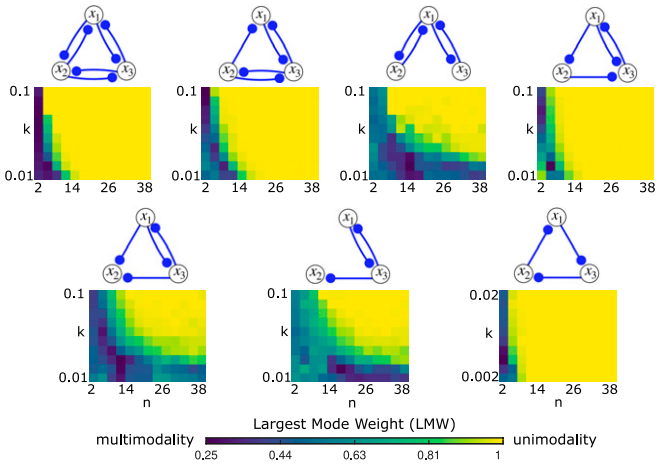

Fig. 6. Size-dependent modality is present for all three-species inhibitory systems (connectivities above the heat maps). As the system size (n) increases, multimodality (dark) transitions to unimodality (yellow), where modality is measured by the LMW of the empirical distribution. This phenomenon is robust to changes in k (weakness of inhibition). *SI Appendix* has further details.

Notice that for $\omega = 1$, inhibition and excitation are given by the same hyperbolic functions as for the two-species systems in Eq. **4**. By using the parameter ω, we extend our analysis with weighing the contribution of excitatory connections.

We first considered seven network connectivities for three-species inhibitory systems (graphs in Fig. 6). These consist of all the connectivities where each species is inhibited by at least one other species, which is a necessary and sufficient condition for the species to stay alive and not die out indefinitely.

For both asymmetric and symmetric inhibitory systems (where symmetry means that $k_{ij} = k_{lm} = k$ for all $i, j, l, m \in \{1, 2, 3\}, i \neq j, l \neq m$), the relationship between the system's modality, the strength of inhibition, and the system size generalizes from systems with two species to three species. More precisely, multimodality is more prevailing when the system size is smaller and when the inhibition between the species is stronger. This is summarized for symmetric systems in Fig. 6 by using the LMW as a measure of unimodality. More precisely, in Fig. 6, we can see that as the system size (n) grows, the system transits from multimodal behavior to unimodal behavior for all the seven connectivities, and this tendency is robust to the parameter k. Furthermore, in agreement with the two-species systems, smaller k (stronger inhibition) widens the multimodal regime of n. Note that the parameter k shapes the stationary distribution of the system, and thus, k can be used to achieve desired separation of different modes and switching times between them.

The dependence of system modality on the parameters k and n can qualitatively be predicted by using the LNA. More precisely, the trend of the LMW and the probability mass inside the positive quadrant P_{in} calculated from the LNA agree in the parameters k and n. For quantitative prediction on the parameter regimes of multimodality, LNA is suitable if an S_{II} motif determines the modality (Fig. 6, *Top*, graph 3, and *Bottom*, graphs 1 and 2); otherwise, the correspondence is qualitative.

We finally extended our analysis to allow mixed excitatory and inhibitory connections. The 94 network connectivities that we obtain this way are illustrated. We used the parameter ω to scale the relative strengths of excitatory connections in the system. For tractability, we fixed $n = 2$ and $k_{ij} = k = 0.01$, $i, j \in \{1, 2, 3\}, i \neq j$ that provided a parametrization where all seven inhibitory systems acquired multimodality.

In Fig. 7, *Middle*, the LMWs of the 94 systems are presented as follows. Each heat map corresponds to one connectivity scheme

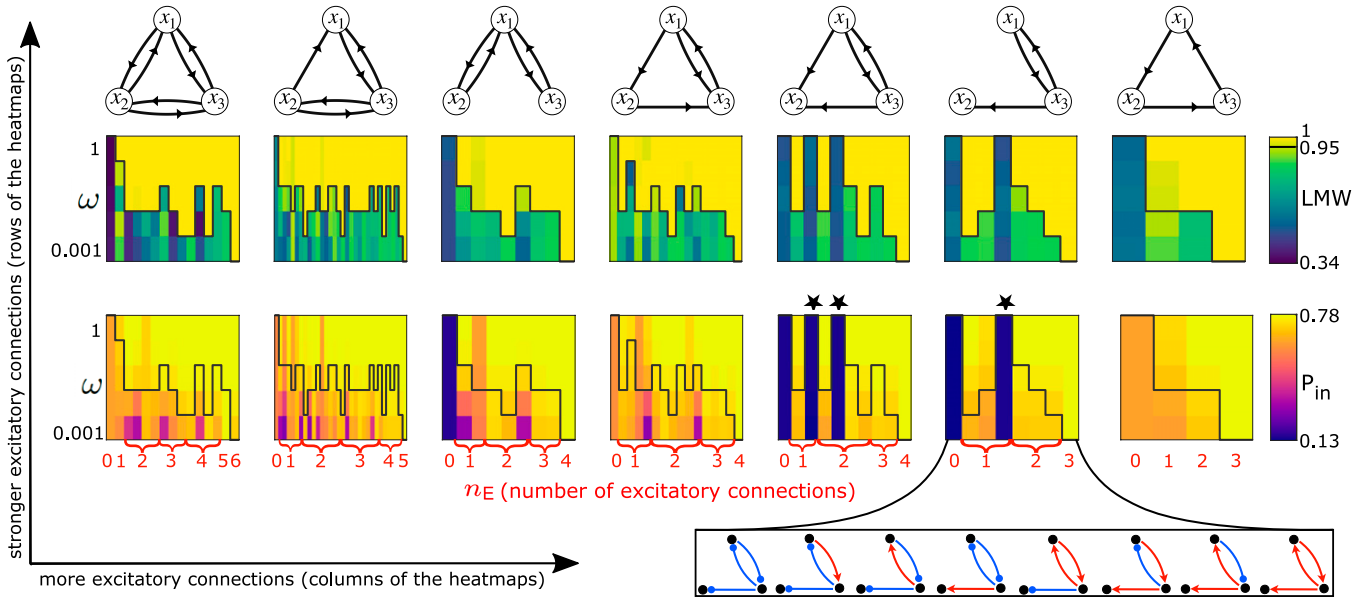

Fig. 7. Multimodality occurs in systems with mixed connectivity only when inhibitory subsystems are dominant. (*Top*) Graph illustration of the seven architectures with three species. (*Middle*) Heat maps of the LMW of the different connectivities (columns of the heat maps) within each architecture and strengths for excitatory connections (ω, rows of the heat maps). (*Bottom*) Heat maps of the probability inside the positive orthant (P_{in}) with the same arrangement for rows and columns within the heat maps as for LMW in *Middle*. The connectivities (columns of the heat map) are not depicted for all architectures but only for the sixth architecture (in the black box at the bottom). Instead, we display the number of excitatory connections (n_{E}) within the connectivities by red numbers that apply both for LMW and the P_{in} heat maps. We use red curly brackets to display n_{E} at once for connectivities with the same number of excitatory connections. The connectivities of all seven architectures are depicted. A black line at LMW $= 0.95$ serves as a marker to distinguish multimodality (when LMW is significantly smaller than one under the line) and unimodality (when LMW is close to one above the line). Multimodality is detected in systems with 1) fully inhibitory connections ($n_{\text{E}} = 0$), 2) mixed connectivity where excitatory connections are weak (ω is small), or 3) two species that have fully inhibitory connections and only have feed-forward excitatory connections to the third species (columns marked by black stars). These general tendencies can be seen from both LMW (*Middle*) gained from the empirical stationary distribution and from P_{in} (*Bottom*) gained analytically from the LNA.

(in the graphs in Fig. 7, *Top*); within one heat map, each row corresponds to one value of ω decreasing from top to bottom, and within one heat map, each column corresponds to a specific network connectivity, where these connectivities are arranged such that fully inhibitory systems gradually change into fully excitatory systems (from left to right). The number of excitatory connections of the connectivities is shown in the x axis of the heat maps in Fig. 7, *Bottom*, see *SI Appendix* for more details on the connectivity.

The results show that if there is at least one inhibitory connection and the contribution of the excitatory connections is weak (ω is small), then the systems acquire multimodality. However, as the excitatory connections become stronger (ω is increasing), multimodal systems almost universally become unimodal. There is one category (columns marked by dark stars) where multimodality persists regardless of the strength of excitatory connections, namely when there is an inhibitory loop between two species and there is only feed-forward excitatory connection to the third species. However, the latter case boils down to the two-species S_{II} system in terms of modality because the third species does not affect the evolution of the two other species; thus, the multimodality arising from the inhibitory subsystem is also unaffected by the third species. In general, we can conclude that three-dimensional systems have diverse modality if excitatory connections are feed forward from or weakly feedback to an inhibitory subsystem.

In Fig. 7, *Bottom*, we present results on the probability inside the positive orthant P_{in} calculated from the LNA. The arrangements of the results are the same as for the LMW in Fig. 7, *Middle*. These results show that P_{in} is a good indicator of whether a system is multimodal. However, as mentioned previously for symmetric inhibitory systems, LNA is not always suitable for determining the parameter regimes (of ω, k, or n) of different modalities. This can be seen from the similar tendencies but different exact coloring of the heat maps of LMW and LNA.

In summary, the results in Figs. 6 and 7 show that the dependence of switching and stable behavior on system size is not a feature of a highly specific biochemical network and can exist in the face of significant parameter variation. The switching behavior relies on the multiple modes appearing close to the natural boundaries of biochemical networks where at least one species becomes extinct. The dependence of this phenomenon on the size is thus intuitive since extinction events are more common in small systems. Our analysis suggests that inhibitory subnetworks are necessary components for the occurrence of switching behavior. This is because they direct the fluctuations of the biochemical networks toward the natural boundaries, allowing the formation of modes in the small system size regime. This trait can be analytically predicted by using LNA.

Discussion

In this paper, we described and analyzed a biochemical motif that produces a stochastic switching behavior regulated by the system's size. Our results rely on the fact that in biological compartments, where reactions occur randomly, the size of the system can have a crucial role in shaping the behavior. Reaction networks that exhibit a stable macroscopic equilibrium can acquire robust switching behavior in the small number limit. This limit typifies small synapses, where the impact of fluctuations and molecular noise has long been recognized as a potential problem for reliable signaling (37, 46, 47). Our proposal turns this problem on its head, suggesting that if breakdown of mass-action kinetics drives bimodal behavior, as happens readily in a number of simple motifs that we have analyzed, then the resulting

system can function as a reliable switch. Moreover, when such a switch is coupled to growth of the compartment, a form of autoregulation emerges that is consistent with the observation that many types of synapse become progressively resistant to further growth as they increase in size (30–34).

There are numerous biochemical pathways that control potentiation and growth of excitatory synapses. Perhaps the most well-known is the CaMKII/protein phosphatase-1 pathway (25, 39, 48, 49), which mediates potentiation following strong synaptic activation and calcium influx. Classic models of this system proposed that CaMKII activates in a switch-like manner, exhibiting macroscopic bimodality in a number of detailed models of the reaction mechanism (11). Notably, the biological relevance of the parameter regime for which the CaMKII concentration shows switch-like behavior has been a subject of debate (26, 40, 50). Studies (7, 11, 13) have shown that the CaMKII phosphorylation can be bistable and thus, fulfills the basic requirements of a switch. However, other studies (40, 51) present contradictory results. Our results provide a potential solution to this controversy by showing that the existence of bistability itself can be sensitive to the absolute quantity of reactants present, which could be in the tens in an intact synapse. This effect is not systematically accounted for or controlled in this extensive prior work.

We would like to stress that there are other known mechanisms that regulate synapse growth and retraction (23, 38) and other membranous compartment regulation that can involve explicit mechanical sensing (52, 53). Thus, the size-dependent switch we describe here is unlikely to represent a unique mechanism in any system, including synapses. Biology often exploits parallel and degenerate mechanisms to ensure robustness and flexibility, so we would expect size-dependent switches to be layered within and interact with distinct mechanisms for controlling compartment growth. The distinguishing feature of the size-dependent switch is that it can operate reliably within very confined subcompartments and possibly, within protein complexes such as postsynaptic densities, where switching mechanisms and size regulation are important (36).

Our results also provide more general understanding of how switches can be identified—or indeed, constructed synthetically—in biochemical signaling networks. We found that inhibitory motifs play a key role in determining size-dependent switching behavior. In two- and three-species systems, we showed that exact stochastic simulations qualitatively agree with a general scheme where the fluctuation of inhibitory systems, corresponding to negative covariance in an LNA, increases the likelihood of extinction events in small systems. Such events can lengthen the dwell time of the system in a nearby region of the state space, resulting in a mode where there is no (macroscopic) equilibrium point.

In light of these results, we hypothesize that this phenomenon holds generally for inhibitory systems, regardless of dimensionality. Moreover, we conjecture that the results extend to systems with different analytic forms for the inhibitory reaction rates beyond Hill functions, provided the geometry of the nullclines in the mean-field description is approximately preserved. Establishing this result without recourse to expensive simulation will require new analytical tools in nonlinear stochastic systems that so far remain out of reach despite decades of research (15, 16, 18, 45, 54–56). Nonetheless, the consistency of the results documented here suggests that size-dependent regulation mechanisms can readily exist in general biochemical systems.

Furthermore, the robustness of the switching transition to parameter variation means that global features, such as survival probability, switching time, and steady-state synapse size, can be tuned. We also note that the number of potential modes in the small system size regime is higher for higher-dimensional systems, allowing for more complex switches with multiple modes. Given that this form of switching cannot be predicted by standard continuous differential equation models that use mass-action kinetics, there is the possibility that such mechanisms have been overlooked in known biochemical pathways.

More conceptually, our model is an example of how qualitative features of microscopic, discrete behavior can propagate to macroscopic scales in a controlled way. Many important biochemical reactions occur among species that are present in low copy numbers due to subcellular compartmentalization, small total cell volumes, or—in the case of DNA—the constraint of operating with a single copy of a molecule within a cell. As a result, cell- or tissue-wide events may be determined by microscopic, discrete, stochastic reactions. Our work provides a simple and likely common class of regulation motifs that can bridge these scales.

Materials and Methods

For simulating the processes of the systems described in this paper, we used Gillespie's stochastic simulation algorithm (19), which is described in more details in *SI Appendix*. The empirical stationary distributions of the systems were calculated from averaging independent realizations of these processes.

The LNA (45), which serves as our analytical tool to estimate the covariance of the stationary distributions without relying on simulations, is described in more detail in *SI Appendix*.

The mode search algorithm applied in this paper in order to determine the LMW as a measure of unimodality is described in *SI Appendix*. This algorithm uses empirical measures of the states in order to assign the states to different modes. The weight of each mode is then calculated as the sum of all probabilities belonging to states within the mode.

Data Availability. Data and code have been deposited in Figshare (https://doi.org/10.6084/m9.figshare.19322696) and GitHub (https://github.com/monikajozsa/synapticswitch).

ACKNOWLEDGMENTS. We acknowledge Andreas Petrides and Glenn Vinnicombe for their help on a preliminary form of the ideas presented here and Michael Rule, Thomas Burger, Mehdi Aghagolzadeh, and Dhruva Raman for technical discussions. This work was supported by European Research Council (ERC) Grant 670645 SWITCHLET (to R.S.) and ERC Grant 716643 FLEXNEURO (to T.O.).

1. T. Eissing *et al.*, Bistability analyses of a caspase activation model for receptor-induced apoptosis. *J. Biol. Chem.* **279**, 36892–36897 (2004).
2. K. L. Ho, H. A. Harrington, Bistability in apoptosis by receptor clustering. *PLoS Comput. Biol.* **6**, e1000956 (2010).
3. S. L. Spencer, P. K. Sorger, Measuring and modeling apoptosis in single cells. *Cell* **144**, 926–939 (2011).
4. J. E. Ferrell Jr., E. M. Machleder, The biochemical basis of an all-or-none cell fate switch in Xenopus oocytes. *Science* **280**, 895–898 (1998).
5. L. Qiao, R. B. Nachbar, I. G. Kevrekidis, S. Y. Shvartsman, Bistability and oscillations in the Huang-Ferrell model of MAPK signaling. *PLOS Comput. Biol.* **3**, 1819–1826 (2007).
6. W. Xiong, J. E. Ferrell Jr., A positive-feedback-based bistable 'memory module' that governs a cell fate decision. *Nature* **426**, 460–465 (2003).
7. J. E. Lisman, A. M. Zhabotinsky, A model of synaptic memory: A CaMKII/PP1 switch that potentiates transmission by organizing an AMPA receptor anchoring assembly. *Neuron* **31**, 191–201 (2001).
8. U. S. Bhalla, R. Iyengar, Emergent properties of networks of biological signaling pathways. *Science* **283**, 381–387 (1999).
9. U. S. Bhalla, P. T. Ram, R. Iyengar, MAP kinase phosphatase as a locus of flexibility in a mitogen-activated protein kinase signaling network. *Science* **297**, 1018–1023 (2002).
10. M. Graupner, N. Brunel, STDP in a bistable synapse model based on CaMKII and associated signaling pathways. *PLOS Comput. Biol.* **3**, e221 (2007).

11. A. M. Zhabotinsky, Bistability in the Ca(2+)/calmodulin-dependent protein kinase-phosphatase system. *Biophys. J.* **79**, 2211–2221 (2000).
12. J. H. Kotaleski, K. T. Blackwell, Modelling the molecular mechanisms of synaptic plasticity using systems biology approaches. *Nat. Rev. Neurosci.* **11**, 239–251 (2010).
13. J. Lisman, S. Raghavachari, Biochemical principles underlying the stable maintenance of LTP by the CaMKII/NMDAR complex. *Brain Res.* **1621**, 51–61 (2015).
14. E. M. Ozbudak, M. Thattai, H. N. Lim, B. I. Shraiman, A. Van Oudenaarden, Multistability in the lactose utilization network of *Escherichia coli*. *Nature* **427**, 737–740 (2004).
15. I. Lestas, J. Paulsson, N. E. Ross, G. Vinnicombe, Noise in gene regulatory networks. *IEEE Trans. Automat. Contr.* **53**, 189–200 (2008).
16. A. Lipshtat, A. Loinger, N. Q. Balaban, O. Biham, Genetic toggle switch without cooperative binding. *Phys. Rev. Lett.* **96**, 188101 (2006).
17. T. S. Gardner, C. R. Cantor, J. J. Collins, Construction of a genetic toggle switch in *Escherichia coli*. *Nature* **403**, 339–342 (2000).
18. D. T. Gillespie, Stochastic simulation of chemical kinetics. *Annu. Rev. Phys. Chem.* **58**, 35–55 (2007).
19. D. T. Gillespie, A general method for numerically simulating the stochastic time evolution of coupled chemical reactions. *J. Comput. Phys.* **22**, 403–434 (1976).
20. U. Alon, *An Introduction to Systems Biology: Design Principles of Biological Circuits* (Chapman & Hall/CRC Computational Biology Series, CRC Press, 2019).
21. J. E. Lisman, A mechanism for memory storage insensitive to molecular turnover: A bistable autophosphorylating kinase. *Proc. Natl. Acad. Sci. U.S.A.* **82**, 3055–3057 (1985).
22. J. Lisman, R. Yasuda, S. Raghavachari, Mechanisms of CaMKII action in long-term potentiation. *Nat. Rev. Neurosci.* **13**, 169–182 (2012).
23. J. Nishiyama, R. Yasuda, Biochemical computation for spine structural plasticity. *Neuron* **87**, 63–75 (2015).
24. J. Y. Chang *et al.*, Camkii autophosphorylation is necessary for optimal integration of ca2+ signals during ltp induction, but not maintenance. *Neuron* **94**, 800–808.e4 (2017).
25. S. J. R. Lee, Y. Escobedo-Lozoya, E. M. Szatmari, R. Yasuda, Activation of CaMKII in single dendritic spines during long-term potentiation. *Nature* **458**, 299–304 (2009).
26. J. M. Bradshaw, Y. Kubota, T. Meyer, H. Schulman, An ultrasensitive Ca^{2+}/calmodulin-dependent protein kinase II-protein phosphatase 1 switch facilitates specificity in postsynaptic calcium signaling. *Proc. Natl. Acad. Sci. U.S.A.* **100**, 10512–10517 (2003).
27. H. Urakubo, M. Sato, S. Ishii, S. Kuroda, In vitro reconstitution of a CaMKII memory switch by an NMDA receptor-derived peptide. *Biophys. J.* **106**, 1414–1420 (2014).
28. F. Engert, T. Bonhoeffer, Dendritic spine changes associated with hippocampal long-term synaptic plasticity. *Nature* **399**, 66–70 (1999).
29. J. I. Arellano, R. Benavides-Piccione, J. Defelipe, R. Yuste, Ultrastructure of dendritic spines: Correlation between synaptic and spine morphologies. *Front. Neurosci.* **1**, 131–143 (2007).
30. M. Matsuzaki, N. Honkura, G. C. R. Ellis-Davies, H. Kasai, Structural basis of long-term potentiation in single dendritic spines. *Nature* **429**, 761–766 (2004).
31. J. T. Trachtenberg *et al.*, Long-term in vivo imaging of experience-dependent synaptic plasticity in adult cortex. *Nature* **420**, 788–794 (2002).
32. C. O'Donnell, M. F. Nolan, M. C. W. van Rossum, Dendritic spine dynamics regulate the long-term stability of synaptic plasticity. *J. Neurosci.* **31**, 16142–16156 (2011).
33. A. Holtmaat, L. Wilbrecht, G. W. Knott, E. Welker, K. Svoboda, Experience-dependent and cell-type-specific spine growth in the neocortex. *Nature* **441**, 979–983 (2006).
34. A. J. Holtmaat *et al.*, Transient and persistent dendritic spines in the neocortex in vivo. *Neuron* **45**, 279–291 (2005).
35. N. Yasumatsu, M. Matsuzaki, T. Miyazaki, J. Noguchi, H. Kasai, Principles of long-term dynamics of dendritic spines. *J. Neurosci.* **28**, 13592–13608 (2008).
36. M. B. Kennedy, Signal-processing machines at the postsynaptic density. *Science* **290**, 750–754 (2000).
37. D. Choquet, A. Triller, The dynamic synapse. *Neuron* **80**, 691–703 (2013).
38. R. Yuste, T. Bonhoeffer, Morphological changes in dendritic spines associated with long-term synaptic plasticity. *Annu. Rev. Neurosci.* **24**, 1071–1089 (2001).
39. J. Lisman, H. Schulman, H. Cline, The molecular basis of CaMKII function in synaptic and behavioural memory. *Nat. Rev. Neurosci.* **3**, 175–190 (2002).
40. P. J. Michalski, The delicate bistability of CaMKII. *Biophys. J.* **105**, 794–806 (2013).
41. K. Obashi, J. W. Taraska, S. Okabe, The role of molecular diffusion within dendritic spines in synaptic function. *J. Gen. Physiol.* **153**, e202012814 (2021).
42. A. Biess, E. Korkotian, D. Holcman, Diffusion in a dendritic spine: The role of geometry. *Phys. Rev. E Stat. Nonlin. Soft Matter Phys.* **76**, 021922 (2007).
43. K. Obashi, A. Matsuda, Y. Inoue, S. Okabe, Precise temporal regulation of molecular diffusion within dendritic spines by actin polymers during structural plasticity. *Cell Rep.* **27**, 1503–1515.e8 (2019).
44. H. Murakoshi, H. Wang, R. Yasuda, Local, persistent activation of Rho GTPases during plasticity of single dendritic spines. *Nature* **472**, 100–104 (2011).
45. N. G. Van Kampen, *Stochastic Processes in Physics and Chemistry* (North Holland, 2007).
46. G. Antunes, E. De Schutter, A stochastic signaling network mediates the probabilistic induction of cerebellar long-term depression. *J. Neurosci.* **32**, 9288–9300 (2012).
47. C. Ribrault, K. Sekimoto, A. Triller, From the stochasticity of molecular processes to the variability of synaptic transmission. *Nat. Rev. Neurosci.* **12**, 375–387 (2011).
48. Y. Zhou *et al.*, Interactions between the NR2B receptor and CaMKII modulate synaptic plasticity and spatial learning. *J. Neurosci.* **27**, 13843–13853 (2007).
49. S. Incontro *et al.*, The CaMKII/NMDA receptor complex controls hippocampal synaptic transmission by kinase-dependent and independent mechanisms. *Nat. Commun.* **9**, 2069 (2018).
50. P. J. Michalski, First demonstration of bistability in CaMKII, a memory-related kinase. *Biophys. J.* **106**, 1233–1235 (2014).
51. M. Ordyan, T. Bartol, M. Kennedy, P. Rangamani, T. Sejnowski, Interactions between calmodulin and neurogranin govern the dynamics of CaMKII as a leaky integrator. *PLOS Comput. Biol.* **16**, e1008015 (2020).
52. D. Kilinc, The emerging role of mechanics in synapse formation and plasticity. *Front. Cell. Neurosci.* **12**, 483 (2018).
53. A. Diz-Muñoz, D. A. Fletcher, O. D. Weiner, Use the force: Membrane tension as an organizer of cell shape and motility. *Trends Cell Biol.* **23**, 47–53 (2013).
54. D. T. Gillespie, The chemical langevin equation. *J. Chem. Phys.* **113**, 297–306 (2000).
55. A. Petrides, G. Vinnicombe, "Understanding the discrete genetic toggle switch phenomena using a discrete 'nullcline' construct inspired by the Markov chain tree theorem" in 2017 IEEE 56th Annual Conference on Decision and Control (CDC) (IEEE, New York, NY, 2017), pp. 1614–1621.
56. A. Petrides, "Advances in the stochastic and deterministic analysis of multistable biochemical networks," PhD thesis, University of Cambridge, Cambridge, United Kingdom (2018).